INORGANIC CHEMISTRY FRONTIERS

RESEARCH ARTICLE

View Article Online
View Journal | View Issue

Cite this: *Inorg. Chem. Front.*, 2024, **11**, 8093

Unusual solvent-regulated inversion of a metal stereocenter in an enantiopure Eu_2L_4 helicate: a new strategy for CPL inversion†

Qing Ma,‡ Sen Yin,‡ Ziye Song, Ting Gao, Pengfei Yan, Yanyan Zhou and Hongfeng Li *

Received 10th September 2024,
Accepted 2nd October 2024

DOI: 10.1039/d4qi02276a

rsc.li/frontiers-inorganic

Developing artificial metal helicates with stimuli-responsive helicity inversion is a significant challenge in functional supramolecular chemistry. However, most reported helicity inversions are based on the synchronous transformation of *P*/*M* conformation and the metal center's Δ/Λ configuration, requiring the overcoming of substantial energy barriers. Herein, we report the first example of Δ/Λ configurational inversion of metal centers independent of the *P*/*M* conformational conversion. The helicate $(NMe_4)_2[Eu_2(\mathbf{L}^{\mathbf{R}})_4]$, maintaining a constant *P* helical conformation, undergoes a local metal center configurational conversion from ΛΛ-$(NMe_4)_2[Eu_2(\mathbf{L}^{\mathbf{R}})_4]$ → ΔΛ-$(NMe_4)_2[Eu_2(\mathbf{L}^{\mathbf{R}})_4]$ → ΔΔ-$(NMe_4)_2[Eu_2(\mathbf{L}^{\mathbf{R}})_4]$ upon increasing the content of $CHCl_3$ in CH_3CN. Associated with the conversion, the inversion of circularly polarized luminescence (CPL) activity took place with the luminescence dissymmetry factor (g_{lum} value) changing from −0.23 to +0.44. The understanding thus gained as to the solvent's impact on local chirality inversion enabled the design of CPL optical switches or sensors based on lanthanide helicates.

Introduction

Helical structures are ubiquitous in biological macromolecules such as DNA and proteins, and the helical chirality (*P* or *M*) plays a crucial role in achieving the given physiological functions.[1–5] When external physiological conditions change, their helical chirality often undergoes inversion. For instance, the typically right-handed B-DNA can be converted to left-handed Z-DNA under conditions such as high salt concentration,[6] biogenic amines,[7] changes in pH or mechanical force,[8,9] which significantly affect their functions in the cell. Inspired by the structural characteristics of biomacromolecules, various artificial molecular systems featuring stimuli-responsive helical inversion have been developed, including organic small molecules,[10,11] polymers, supramolecular polymers,[12–14] and metal complexes.[15–19] Chirality inversion usually results in the switching of properties, such as the selectivity of asymmetric catalysis,[20,21] the capability of chiral recognition,[22–25] and chiroptical activities.[26–29]

Since Lehn reported metal helicates based on poly(2,2′-bipyridine),[30] chiral helicates have been developed for applications in targeted therapy,[31] asymmetric catalysis, and chiroptical studies.[32–34] Dynamic regulation of helicity inversion would undoubtedly lead to new breakthroughs in these research areas. In helical complexes, chiral inversion typically involves the simultaneous conversion of helical conformation (*P*/*M*) and the metal center's (Δ/Λ) configuration.[35–39] However, this simultaneous conversion necessitates overcoming a substantial energy barrier, significantly hindering the development of helicates as platforms for chirality inversion. Designing helicates with localized Δ/Λ or *P*/*M* chirality reversal is anticipated to significantly reduce the inversion energy barrier, opening new avenues for exploring their potential.

Introducing lanthanide metals with greater coordination flexibility into helicates can be considered as an effective solution for achieving localized Δ/Λ-configurational reversal. Compared to transition metals, the variable coordination geometry and lack of coordination directionality of Ln(III) ions allow for more freedom of ligand rearrangement during Δ/Λ-configurational reversal. Additionally, the helicity inversion of luminescent lanthanide helicates can induce changes in the chiroptical properties, such as the inversion of circularly polarized luminescence (CPL) signals, expanding their applications in chiroptical switches, optical storage, information encryption, and sensing.[40] Currently, there are no reported examples of controlling the chiral reversal of enantiopure lanthanide helicates.

Key Laboratory of Functional Inorganic Material Chemistry, Ministry of Education, School of Chemistry and Materials Science Heilongjiang University, 74 Xuefu Road, Harbin 150080, China. E-mail: lihongfeng@hlju.edu.cn

†Electronic supplementary information (ESI) available. CCDC 2353626. For ESI and crystallographic data in CIF or other electronic format see DOI: https://doi.org/10.1039/d4qi02276a

‡These authors contributed equally to this work.

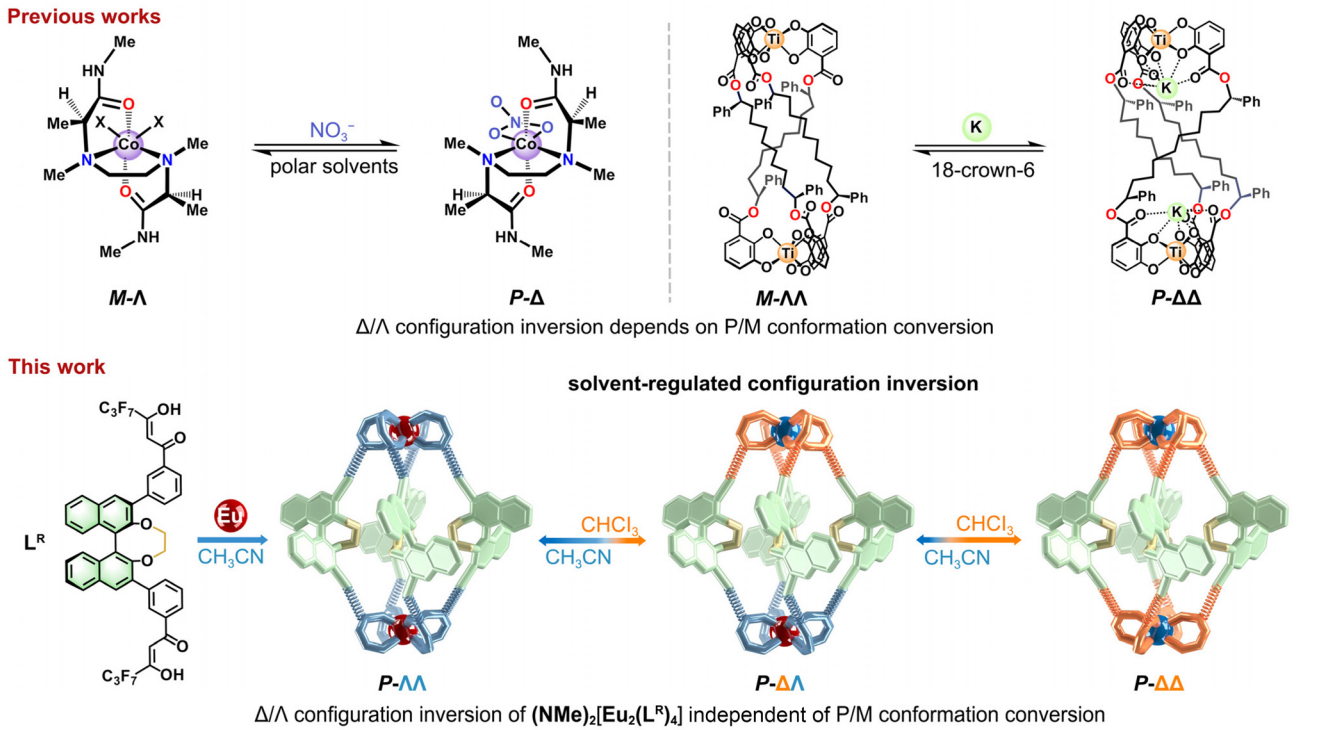

Scheme 1 Previous works: the reported examples of the synchronous inversion of Δ/Λ configuration and *P*/*M* helix conformation.[38,39] This work: the solvent-regulated Δ/Λ metal center configuration inversion process of the helicate $(NMe_4)_2Eu_2(L^R)_4$ while maintaining its *P* helical conformation.

To achieve local Δ/Λ configurational inversion while restricting *P*/*M* conformational conversion, the chiral β-diketonate ligands (L^R), featuring a "fixed" configurational chirality (derived from *R*-binaphthol) and moderate rotation flexibility, were designed (Scheme 1). The resulting helicate $(NMe_4)_2[Eu_2(L^R)_4]$ features solvent-regulated metal stereocenter Δ/Λ configurational inversion that was independent of *P*/*M* helical conformation conversion. Comprehensive spectroscopic characterization combined with DFT calculations and weak interaction analysis using the Independent Gradient Model (IGM) reveals the influence of the counterion on configuration reversal. More importantly, the CPL inversion has also been realized along with this local Δ/Λ conversion.

Results and discussion

Assembly and structure of $(NMe_4)_2[Eu_2(L^R)_4]$

The synthetic procedures of the ligands ($L^{R/S}$) and their characterization through ESI-TOF-MS and ^1H, ^{13}C, and ^{19}F NMR are given in the ESI (Scheme S1 and Fig. S1–S12†). To obtain the $(NMe_4)_2[Eu_2(L^R)_4]$ helicate, the ligand L^R was assembled with $Eu(OTf)_3$ in a 2 : 1 stoichiometric ratio with tetramethylammonium hydroxide (NMe_4OH) as the base in CH_3CN. The high quality, block-shaped crystals suitable for single crystal X-ray analysis were obtained by slow evaporation of the acetonitrile/1,4-dioxane solution of $(NMe_4)_2[Eu_2(L^R)_4]$. The crystal structure analysis confirmed the formation of a quadruple-stranded dinuclear helicate (Fig. 1). $(NMe_4)_2[Eu_2(L^R)_4]$ crystallized in the chiral space group $P42_12$. In each helicate, the *R*-BINOL spacer imparts the assembly with *P*-helical chirality and homochiral ΔΔ configuration to the two metal centers. In the ligands, there are five dihedral angles generating from the BINOL spacer (α = −67.15°), the binaphthyl and benzene ring

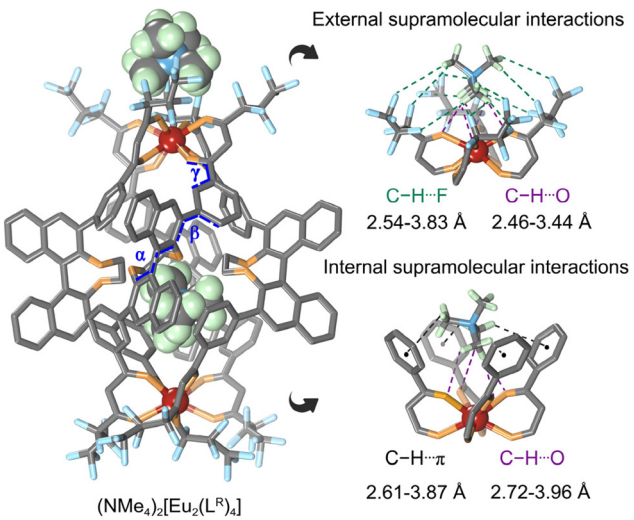

Fig. 1 X-ray single crystal structure of the helicate $(NMe_4)_2[Eu_2(L^R)_4]$, and partially enlarged views of the multiple supramolecular interactions C−H···F, C−H···O and C−H···π between the counterions and the helicate (color code for Eu: red, C: gray, N: blue, F: cyan, H: green, and O: orange). Hydrogen atoms on the helicate and external solvent molecules have been omitted for clarity.

(β = −51.39°), and the benzene ring and diketone unit (γ = −27.90°).

The formation of the helicate results in a large internal cavity, with a calculated volume of 217 Å^3, as determined using the MoloVol program (Fig. S34†).[41] In $(NMe_4)_2[Eu_2(\mathbf{L^R})_4]$, the internal cavity encapsulates one molecular counter cation $(NMe_4)^+$, positioned near one side of the Eu^{3+} ion. The remaining $(NMe_4)^+$ resides within the cavity formed by the four heptafluorinated chains on the helicate's exterior, engaging in strong C–H···F hydrogen bonding interactions. Notably, the distribution of these counterions near the Eu^{3+} ions effectively balances the negative charge from the ligands. As shown by the weak interaction markings in Fig. 1, multiple C–H···O and C–H···π interactions exist between $(NMe_4)^+$ and the ligands within the helicate, with distances ranging from 2.72–3.96 Å and 2.61–3.87 Å, respectively. The counterion outside the helicate exhibits multiple C–H···F hydrogen bonding interactions with the ligands, with distances ranging from 2.54–3.83 Å. Therefore, we believe that the electrostatic interactions, hydrogen bonding, and C–H···π interactions between $(NMe_4)^+$ and the helicate play crucial roles in compensating for the entropy reduction during the assembly processes.

Solvent-regulated inversion of Δ/Λ configuration and CPL in $(NMe_4)_2[Eu_2(\mathbf{L^R})_4]$

To investigate the solvent-dependent dynamic helicity reversal, the solution structure of the complex was first characterized using high-resolution electrospray ionization mass spectrometry (ESI-TOF-MS) and ^{1}H NMR spectroscopy. ESI-TOF-MS confirmed the preservation of the quadruple-stranded helical structure of the complexes after dissolving freshly prepared crystals of $(NMe_4)_2[Eu_2(\mathbf{L^R})_4]$ (Fig. S13†). The presence of a single diffusion band in diffusion-ordered NMR spectroscopy (DOSY) suggests the formation of a single species (Fig. 2b). The hydrodynamic radius (7.25 Å) estimated from the diffusion coefficient (D = 8.0 × 10^{-6} cm^2 s^{-1}) aligns with the size of the helicate determined from single-crystal X-ray diffraction analysis. However, the ^{1}H NMR measurements contradict the existence of a single species, revealing two sets of resonance signals as depicted in Fig. 2b. For example, the methylene signal H^k associated with the diketonate units splits into two distinct signals, with an integration ratio of H^{k1} (δ, −4.0 ppm) : H^{k2} (δ, −4.9 ppm) = 1 : 1.3 (Fig. 2b). This finding indicates the presence of at least two species in CD_3CN. First, the presence of a pair of enantiomers for the helicate can be excluded due to the *R* configuration of the binaphthyl unit being locked by the ethylene group. However, within a single dinuclear helicate, each metal stereocenter can adopt either a Δ or Λ configuration, leading to a maximum of three possible diastereoisomers: ΔΔ-$(NMe_4)_2[Eu_2(\mathbf{L^R})_4]$ (H-ΔΔ), ΛΛ-$(NMe_4)_2[Eu_2(\mathbf{L^R})_4]$ (H-ΛΛ), and ΔΛ-$(NMe_4)_2[Eu_2(\mathbf{L^R})_4]$ (H-ΔΛ). Upon re-examination of the ^{1}H NMR spectrum, a subtle shoulder peak near H^{k2} at δ = −5.0 ppm was observed (labeled as H^{k3}). Therefore, the three sets of H^{k1-k3} signals observed in the ^{1}H NMR spectrum likely indicate a dynamic equilibrium between these three diastereoisomers.

The presence of diastereoisomeric mixtures in the helicate was further confirmed by CD and CPL spectroscopy experiments. As shown in Fig. 2d, the CD spectrum of $(NMe_4)_2[Eu_2(\mathbf{L^R})_4]$ exhibits two distinct Cotton effects in the wavelength ranges of 250–287 nm and 287–370 nm, corresponding to the π–π* transition of the binaphthyl group and the ILCT transition of the ligand, respectively. The negative Cotton effect at λ_{max} = 262 nm aligns with the *R* configuration of the binaphthyl group.[42] Meanwhile, the negative exciton couplet observed for the ligand's transition in the 287–370 nm range indicates a Δ configuration at the metal center and a *P* helical conformation of the helicate,[43] consistent with the crystal structure analysis. Interestingly, the configurational deductions based on CPL spectrum analysis contradict those derived from CD analysis. The negative and positive signals at the $^5D_0 \rightarrow {}^7F_1$ (594 nm) and $^5D_0 \rightarrow {}^7F_2$ (612 nm) transitions, respectively (Fig. 2e), indicate a Λ configuration for the Eu^{3+} ion.[44–46] This discrepancy in the metal center configurations inferred from CD and CPL spectra is a unique phenomenon not previously observed. We propose that this conflict can be explained rationally by considering their distinct chiroptical origins. The exciton coupling pattern observed in the circular dichroism (CD) spectrum is related to the rotational strengths of non-degenerate excitonic states (R^A and R^B) of the chromophore, which can be defined using eqn (1):[47]

$$R^{A/B} = \pm \frac{E\mu^2 r}{4\hbar}(\sin\theta \cdot \sin\theta' \cdot \sin\tau) \quad (1)$$

where τ represents the included angle between the two dipole moments (μ_A and μ_B) of spatially proximate chromophores, and θ and θ' are the angles between μ_A, μ_B and $\hat{r}$ ($\hat{r}$ is the vector connecting the centre of gravity of the chromophores). By virtue of TD-DFT, the angles (τ, θ and θ') in $(NMe_4)_2[Eu_2(\mathbf{L^R})_4]$ were calculated and are listed in Table S2.† According to eqn (1), the R^A values are positive for both H-ΛΛ and H-ΔΔ isomers (the details are described in the ESI†), despite the inverse configurations of the metal centers. The positive value indicates a negative exciton couplet, which is consistent with the observed pattern in the CD spectrum (Fig. 2d). This finding demonstrates that the exciton coupling pattern in helicates remains consistent as long as the *P* helical conformation remains unchanged, regardless of the Δ/Λ configurational inversion. Consequently, employing the empirical rule of exciton coupling patterns in CD spectra to deduce the configuration of the metal stereocenter is not effective in this study. This specific case emphasizes the need for caution when correlating the configuration of the metal center with CD spectra, despite the rule's proven effectiveness in most instances.

Conversely, the circularly polarized luminescence (CPL) spectral pattern is reported to solely correspond to the configuration of the Ln^{3+} ion. Thus, the Λ configuration deduced from the CPL spectrum likely arises from an excess of Λ- over Δ-configurational moieties in the mixture of ΔΔ-$(NMe_4)_2[Eu_2(\mathbf{L^R})_4]$, ΛΛ-$(NMe_4)_2[Eu_2(\mathbf{L^R})_4]$, and ΔΛ-$(NMe_4)_2[Eu_2(\mathbf{L^R})_4]$.

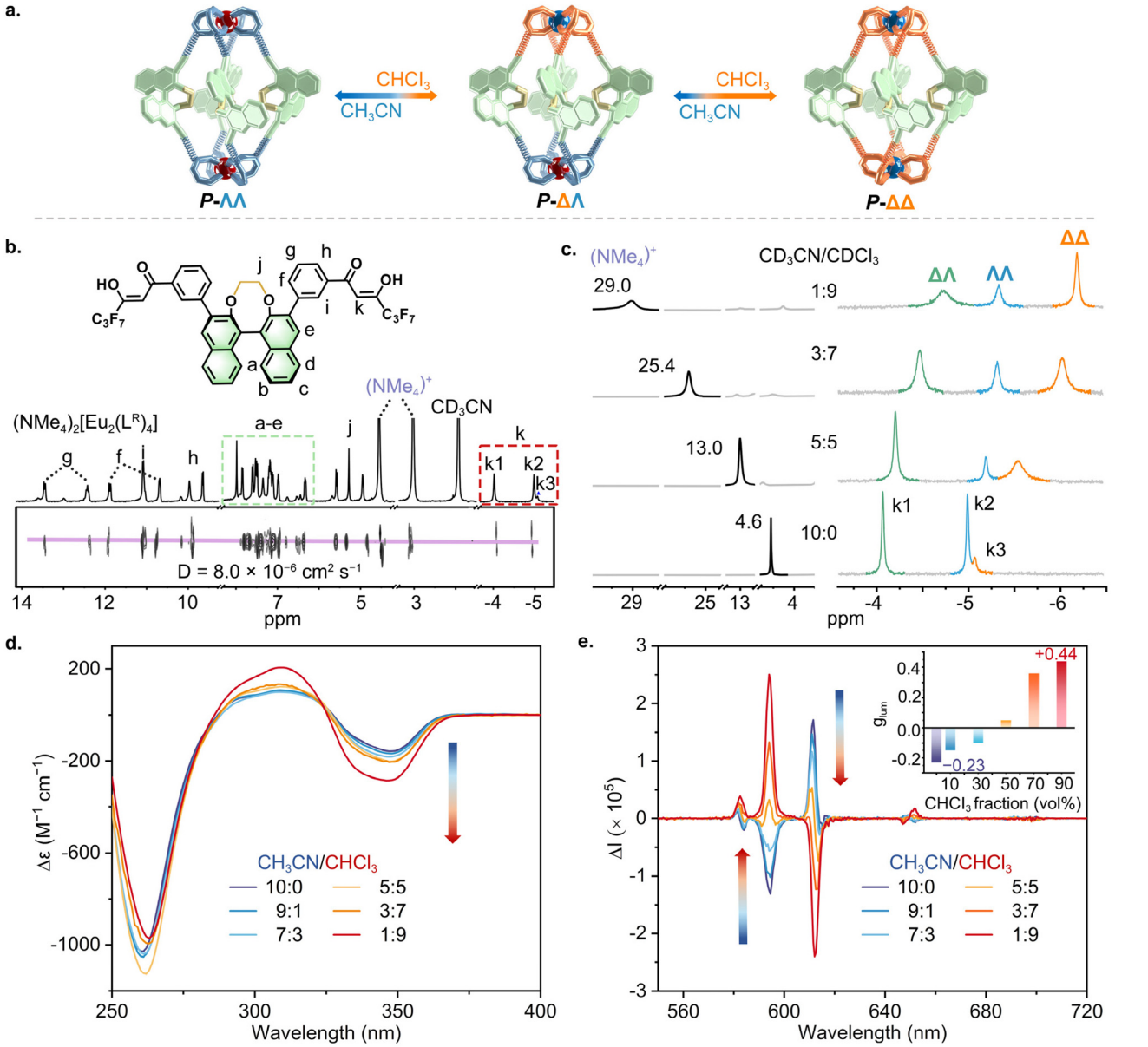

Fig. 2 Solvent-regulated inversion of the Δ/Λ configurations and CPL in $(NMe_4)_2[Eu_2(L^R)_4]$. (a) The inversion process (ΛΛ ⇌ ΔΛ ⇌ ΔΔ) in the helicate $(NMe_4)_2[Eu_2(L^R)_4]$. (b) ^{1}H NMR and ^{1}H DOSY spectra of $(NMe_4)_2[Eu_2(L^R)_4]$ (400 MHz, 295 K, CD_3CN). (c) Partial ^{1}H NMR spectral changes of $(NMe_4)_2[Eu_2(L^R)_4]$ with the increase of $CDCl_3$ content in CD_3CN (400 MHz, 295 K, $CD_3CN/CDCl_3$ = v/v): $CD_3CN/CDCl_3$ = 10 : 0, $H^{k1} : H^{k2} : H^{k3}$ = 0.45 : 0.44 : 0.11; $CD_3CN/CDCl_3$ = 5 : 5, $H^{k1} : H^{k2} : H^{k3}$ = 0.49 : 0.15 : 0.36; $CD_3CN/CDCl_3$ = 3 : 7, $H^{k1} : H^{k2} : H^{k3}$ = 0.39 : 0.22 : 0.39; $CD_3CN/CDCl_3$ = 1 : 9, $H^{k1} : H^{k2} : H^{k3}$ = 0.39 : 0.21 : 0.40. (d) CD and (e) CPL spectral changes of $(NMe_4)_2[Eu_2(L^R)_4]$ with the increase of $CHCl_3$ content in CH_3CN (v/v, c = 2.5 × 10^{-6} M); the inset graph shows the increasing trend of the g_{lum} value of $(NMe_4)_2[Eu_2(L^R)_4]$ at 594 nm during the solvent regulation process.

To elucidate the structural transformation from a H-ΛΛ configuration in the crystal to a diastereoisomeric mixture in solution, we reexamined the crystal structure of $(NMe_4)_2[Eu_2(L^R)_4]$. We suggest that supramolecular interactions between the counterions and the helicate may play a crucial role in this configurational conversion. For example, beyond electrostatic interactions, twelve hydrogen bonds (C–H···O) and C–H···π interactions exist between the inner $(NMe_4)^+$ and the helicate (Fig. 1). The $(NMe_4)^+$ located outside the helicate also exhibits multiple hydrogen bonding (C–H···O and C–H···F) interactions with the oxygen and fluorine atoms of the ligands. Therefore, we propose that solvation of the counterions and the helicate in CH_3CN may disrupt or weaken these interactions, leading to the observed transformation. This implies that strengthening ion pair interactions by adding weak polar solvents into CH_3CN will result in conversion from Λ to Δ.

This inference is supported by the varying proportions of the three components, H-ΔΔ, H-ΛΛ, and H-ΔΛ, in different polar solvents. Upon increasing the content of weakly polar

$CDCl_3$ in CD_3CN, the integration ratio of H^k shifts from $H^{k1} : H^{k2} : H^{k3}$ = 0.45 : 0.44 : 0.11 in pure CD_3CN to 0.39 : 0.21 : 0.40 in $CD_3CN/CDCl_3$ = 1 : 9, indicating the presence of diastereoisomeric interconversion (Fig. 2c). This conversion is also reflected in the intensity variation of the molar extinction coefficient in the CD spectra, where $\Delta\varepsilon$ (λ = 347 nm) increases from −160 M^{-1} cm^{-1} in CH_3CN to −286 M^{-1} cm^{-1} at a $CD_3CN/CDCl_3$ ratio of 1 : 9 (Fig. 2d). The increased $\Delta\varepsilon$ suggests a higher proportion of the Δ-configurational moiety within the diastereoisomeric mixture. This configurational reversal is more directly observed in the inversion of CPL signals. For example, the g_{lum} value of −0.23 at 594 nm in CH_3CN is reversed to +0.44 in $CH_3CN/CHCl_3$ = 1 : 9 (Fig. 2e, orange line), indicating a transformation from a Λ-dominated to a Δ-dominated diastereoisomeric composition.

Combining ^1H NMR and CPL spectra, we infer that the proton H^{k3} with gradually increasing integration corresponds to the homochiral H-ΔΔ isomer, while the H^{k2} with the reduced integration corresponds to the homochiral H-ΛΛ. The remaining H^{k1} is attributed to the pseudo-*meso* H-ΔΛ, as its content remains relatively constant, with only a slight decrease from 0.45 to 0.39, consistent with the transformation process of H-ΛΛ → H-ΔΛ → H-ΔΔ. We propose that the configuration reversal process is driven by the enhanced ion pair interactions resulting from the increased content of weakly polar $CHCl_3$. ESI-TOF-MS provides evidence for ion pair formation in a mixed solvent of $CH_3CN/CHCl_3$, where a peak at m/z = 4132.4870 corresponding to the $[(NMe_4)^+ + Eu_2(\mathbf{L^R})_4]^-$ ion was observed (Fig. S21†). Furthermore, the H–F correlation signals in the HOESY spectrum support the presence of ion pair interactions between $(NMe_4)^+$ and the heptafluoroalkyl chains (Fig. S22†). Additionally, the helicate exhibits distinct luminescence efficiencies in CH_3CN and $CH_3CN/CHCl_3$ = 1 : 9, with luminescence quantum yields of 19% and 24%, respectively (Fig. S32 and S33†), and detailed photophysical parameters are summarized in Table S1.† In conclusion, this rare example of solvent-regulated inversion of Δ ↔ Λ configuration and CPL signals, independent of $P \leftrightarrow M$ helical reversal, provides valuable insights into the dynamic regulation of multinuclear assemblies and the development of CPL optical switches.

DFT computational studies and IGM analysis

To investigate the role of solvent in regulating the supramolecular interactions between $(NMe_4)^+$ and $[Eu_2(\mathbf{L^R})_4]^{2-}$, thereby controlling the Δ/Λ configuration inversion, DFT calculations were performed to assess the system energy of the helicate in three diastereoisomers: H-ΛΛ, H-ΔΛ, and H-ΔΔ. Details of the DFT calculations are provided in the ESI.† Initial coordinates for H-ΔΔ were obtained from the X-ray structure, while coordinates for H-ΔΛ and H-ΛΛ were generated by reversing the Δ configuration of one or two Eu^{3+} ions in the H-ΔΔ helicate. Initially, the three structures were optimized without the counterion $(NMe_4)^+$ to model the situation of the helicate in CH_3CN, where the ion pair should dissociate to an extreme due to the excellent solvation capability of CH_3CN, as evidenced by the identical chemical shifts of free $(NMe_4)^+$ and those within the complex (Fig. 2b and S18†).

The optimized structures and calculated system energies are depicted in Fig. 3a and S37.† Compared to the single-crystal structure, the dihedral angle (α') of the binaphthyl moiety in H-ΔΔ increases from −63.56° to −68.28°. Simultaneously, the heptafluoroalkyl chains in H-ΔΔ approach each other, with the C–H···F distance shortening from 4.12 Å to 2.54 Å. In contrast to H-ΔΔ, H-ΛΛ achieves a complete reversal of configuration by twisting the dihedral angle (γ') between the biphenyl and diketonate unit from −26.15° to +34.40°. This reversal process also increases the Eu···Eu distance from 14.34 Å in H-ΔΔ to 15.46 Å. In the heterochiral H-ΔΛ, the Eu···Eu distance is shortened to 14.32 Å with dihedral angles (γ') of −27.34° and +29.71°, respectively (Fig. S37†). Precise energy calculations reveal that H-ΛΛ possesses the lowest energy compared to H-ΔΛ and H-ΔΔ, which aligns with the prediction of the Λ-configurational excess of $(NMe_4)_2[Eu_2(\mathbf{L^R})_4]$ in CH_3CN inferred from chiroptical analysis.

ESI-TOF-MS, NMR, and CPL spectra have established a correlation between configuration reversal and the enhancement of ion pair interactions. Therefore, geometry optimizations and energy calculations were further performed for the three helicates (H-ΛΛ, H-ΔΛ, and H-ΔΔ) in the presence of the counterion $(NMe_4)^+$. The results indicate that H-ΔΔ exhibits lower energies than H-ΛΛ and H-ΔΛ, suggesting that H-ΔΔ is the thermodynamically dominant component in the mixed solvent. This result is consistent with the observed configuration reversal in $CH_3CN/CHCl_3$.

Considering the influence of the counterion on configuration reversal, we propose that the strength of interactions between $(NMe_4)^+$ and Δ- and Λ-configurational isomers should differ. To explore this further, we performed visualization analyses of the weak interactions using the Independent Gradient Model (IGM).[48,49] The results revealed a significant presence of green regions between $(NMe_4)^+$ and the helicate, indicating the presence of multiple weak intermolecular interactions (Fig. 3c). To quantitatively investigate and visualize these supramolecular interactions, Hirshfeld surface analysis was conducted. This analysis highlighted strong contacts between $(NMe_4)^+$ and the helicate, predominantly driven by C–H···F and C–H···O interactions. It was found that H-ΔΔ exhibits tighter contacts with $(NMe_4)^+$ compared to H-ΛΛ, evidenced by the shorter N···Eu distance (4.73 Å for H-ΔΔ and 4.83 Å for H-ΛΛ) and the larger C–H···O contribution (25.5% for H-ΔΔ and 20.8% for H-ΛΛ) (Fig. 3b and c). This result implies that the formation of the $(NMe_4)^+$/H-ΔΔ ion pair is more thermodynamically favourable than that of the $(NMe_4)^+$/H-ΛΛ analogue. Therefore, based on the aforementioned DFT calculations, IGM, and Hirshfeld surface analyses, the solvent-dependent formation of ion pairs and the discriminated thermodynamic stability of the diastereoisomeric partners are the primary factors responsible for the observed dynamic configuration reversal.

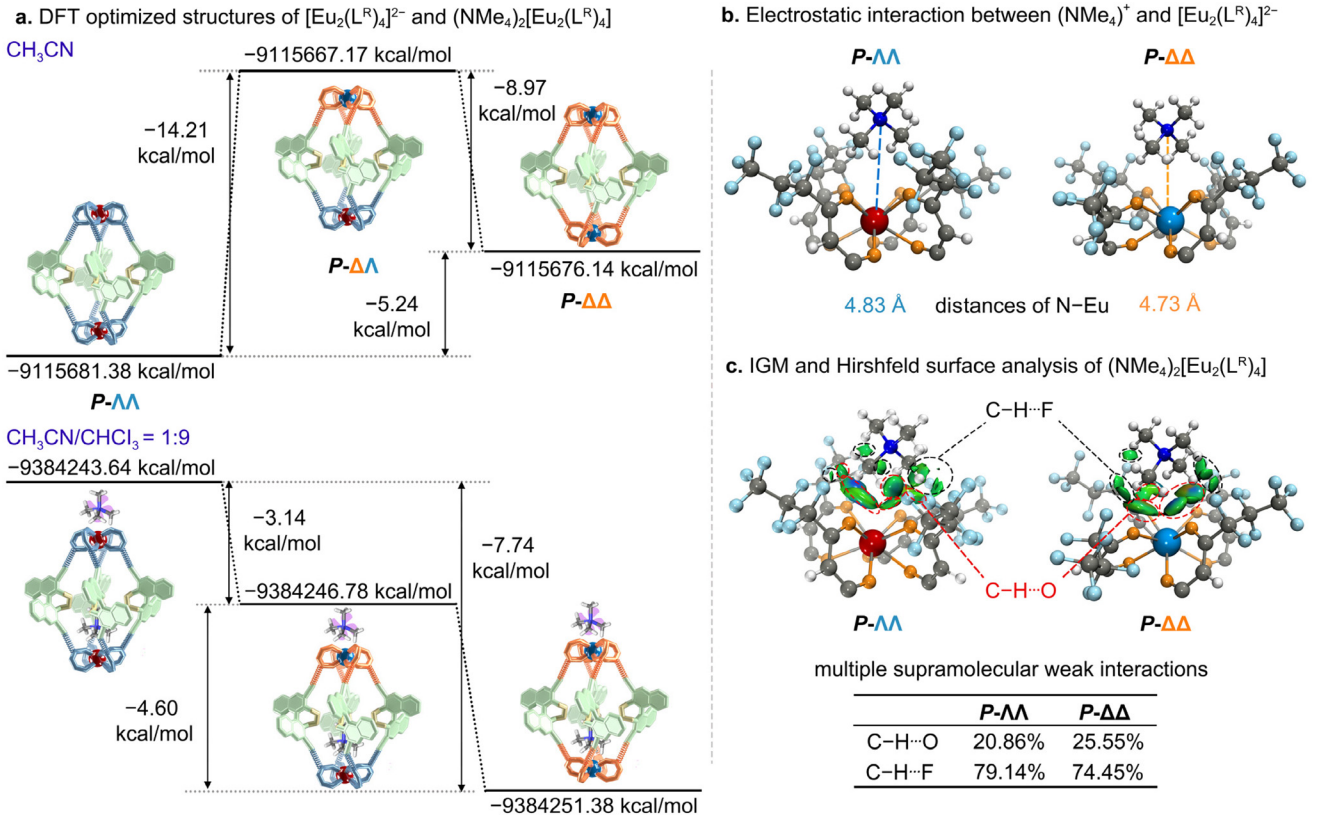

	P-ΛΛ	P-ΔΔ
C−H···O	20.86%	25.55%
C−H···F	79.14%	74.45%

Fig. 3 DFT-optimized structures (energies are given in kcal mol^{-1}), IGM and Hirshfeld surface analysis of $(NMe_4)_2[Eu_2(L^R)_4]$. (a) DFT-optimized structures of H-ΛΛ, H-ΔΛ and H-ΔΔ under the different solvent conditions of CH_3CN and $CH_3CN/CHCl_3$ = 1 : 9. (b) The distances of electrostatic interactions between $(NMe_4)^+$ and DFT-optimized helicates (H-ΛΛ and H-ΔΔ) in $CH_3CN/CHCl_3$ = 1 : 9. (c) IGM and Hirshfeld surface analysis of the weak interactions C−H···O, C−H···F of H-ΛΛ and H-ΔΔ in $CH_3CN/CHCl_3$ = 1 : 9.

Conclusion

This work presents the first example of a metal helicate exhibiting Δ/Λ configuration inversion at the metal stereocenter, independent of *P*/*M* helical conformation reversal. This achievement was realized by employing a strategy that combines a conformationally "fixed" binaphthyl group with a "dynamic" lanthanide coordination unit, thereby inverting the local chirality of the helicate. This strategy not only reduces the difficulty of regulating the metal center configuration inversion but also enables the ground-state absorption and lanthanide excited-state emission to exhibit opposite chiroptical changes, which is unattainable in helicates undergoing Δ/Λ and *P*/*M* simultaneous reversals. These findings offer a viable strategy for dynamically regulating local chirality reversal in helicates while highlighting the unique potential of lanthanide supramolecules as CPL switches due to their significant CPL signal variations (Δg_{lum} = 0.67 for this work).

Author contributions

H. F. L. conceived and supervised the project. Q. M. performed the experiments and analysed the data. S. Y. assisted with the synthesis of compounds. S. Y. and Z. Y. S. collected diffraction data and solved and refined the X-ray crystal structures. H. F. L., Y. Y. Z., T. G. and P. F. Y. reviewed and edited the paper. All authors contributed to the final draft of the paper.

Data availability

The data that support the findings of this study are available in the ESI† of this article.

Conflicts of interest

The authors declare no conflict of interest.

Acknowledgements

This work was financially supported by the National Natural Science Foundation of China (no. 52273263, 52203219 and 52073080), the Scientific Research Project of Basic Scientific Research Operating Expenses of Colleges and Universities in

Heilongjiang Province (2021-KYYWF-0029 and 2021-KYYWF-0041), and the Heilongjiang Provincial Natural Science Foundation Joint Guidance Project no. LH2023B022.

References

1 T. J. Richmond and C. A. Davey, The structure of DNA in the nucleosome core, *Nature*, 2003, **423**, 145–150.
2 G. A. Armeev, A. S. Kniazeva, G. A. Komarova, M. P. Kirpichnikov and A. K. Shaytan, Histone dynamics mediate DNA unwrapping and sliding in nucleosomes, *Nat. Commun.*, 2021, **12**, 2387.
3 Z. Wang, D. Zhang, X. Qiu, H. Inuzuka, Y. Xiong, J. Liu, L. Chen, H. Chen, L. Xie, H. Ü. Kaniskan, X. Chen, J. Jin and W. Wei, Structurally specific Z-DNA proteolysis targeting chimera enables targeted degradation of adenosine deaminase acting on RNA 1, *J. Am. Chem. Soc.*, 2024, **146**, 7584–7593.
4 Y. M. Kang, J. Bang, E. H. Lee, H. C. Ahn, Y. J. Seo, K. K. Kim, Y. G. Kim, B. S. Choi and J. H. Lee, NMR spectroscopic elucidation of the B-Z transition of a DNA double helix induced by the Zα domain of human ADAR1, *J. Am. Chem. Soc.*, 2009, **131**, 11485–11491.
5 H. A. Rothan, K. Arora, J. P. Natekar, P. G. Strate, M. A. Brinton and M. Kumar, Z-DNA-binding protein 1 is critical for controlling virus replication and survival in west nile virus encephalitis, *Front. Microbiol.*, 2019, **10**, 2089.
6 F. M. Pohl and T. M. Jovin, Salt-induced co-operative conformational change of a synthetic DNA: equilibrium and kinetic studies with poly(dG-dC), *J. Mol. Biol.*, 1972, **67**, 375–396.
7 A. Parkinson, M. Hawken, M. Hall, K. J. Sanders and A. Rodger, Amine induced Z-DNA in poly(dG-dC)·poly(dG-dC): circular dichroism and gel electrophoresis study, *Phys. Chem. Chem. Phys.*, 2000, **2**, 5469–5478.
8 A. D'Urso, A. Mammana, M. Balaz, A. E. Holmes, N. Berova, R. Lauceri and R. Purrello, Interactions of a tetraanionic porphyrin with DNA: from a Z-DNA sensor to a versatile supramolecular device, *J. Am. Chem. Soc.*, 2009, **131**, 2046–2047.
9 J. Yi, S. Yeou and N. K. Lee, DNA bending force facilitates Z-DNA formation under physiological salt conditions, *J. Am. Chem. Soc.*, 2022, **144**, 13137–13145.
10 X. Jiang, Y. K. Lim, B. J. Zhang, E. A. Opsitnick, M. H. Baik and D. Lee, Dendritic molecular switch: chiral folding and helicity inversion, *J. Am. Chem. Soc.*, 2008, **130**, 16812–16822.
11 Y. Liu, Q. Zhang, S. Crespi, S. Chen, X. K. Zhang, T. Y. Xu, C. S. Ma, S. W. Zhou, Z. T. Shi, H. Tian, B. L. Feringa and D. H. Qu, Motorized macrocycle: a photo-responsive host with switchable and stereoselective guest recognition, *Angew. Chem., Int. Ed.*, 2021, **60**, 16129–16138.
12 H. Jiang, Y. Jiang, J. Han, L. Zhang and M. Liu, Helical nanostructures: chirality transfer and a photodriven transformation from superhelix to nanokebab, *Angew. Chem., Int. Ed.*, 2019, **58**, 785–790.
13 D. Hirose, A. Isobe, E. Quiñoá, F. Freire and K. Maeda, Three-state switchable chiral stationary phase based on helicity control of an optically active poly(phenylacetylene) derivative by using metal cations in the solid state, *J. Am. Chem. Soc.*, 2019, **141**, 8592–8598.
14 K. Shimomura, T. Ikai, S. Kanoh, E. Yashima and K. Maeda, Switchable enantioseparation based on macromolecular memory of a helical polyacetylene in the solid state, *Nat. Chem.*, 2014, **6**, 429–434.
15 S. Akine, S. Hotate and T. Nabeshima, A molecular leverage for helicity control and helix inversion, *J. Am. Chem. Soc.*, 2011, **133**, 13868–13871.
16 S. Akine, S. Sairenji, T. Taniguchi and T. Nabeshima, Stepwise helicity inversions by multisequential metal exchange, *J. Am. Chem. Soc.*, 2013, **135**, 12948–12951.
17 J. Gregoliński and J. Lisowski, Helicity inversion in lanthanide(III) complexes with chiral nonaaza macrocyclic ligands, *Angew. Chem., Int. Ed.*, 2006, **45**, 6122–6126.
18 S. Sairenji, S. Akine and T. Nabeshima, Response speed control of helicity inversion based on a "regulatory enzyme"-like strategy, *Sci. Rep.*, 2018, **8**, 137.
19 S. A. Ikbal, P. Zhao, M. Ehara and S. Akine, Acceleration and deceleration of chirality inversion speeds in a dynamic helical metallocryptand by alkali metal ion binding, *Sci. Adv.*, 2023, **9**, eadj5536.
20 J. Jiang, Y. Meng, L. Zhang and M. Liu, Self-assembled single-walled metal-helical nanotube (M-HN): creation of efficient supramolecular catalysts for asymmetric reaction, *J. Am. Chem. Soc.*, 2016, **138**, 15629–15635.
21 M. Suginome, T. Yamamoto, Y. Nagata, T. Yamada and Y. Akai, Catalytic asymmetric synthesis using chirality-switchable helical polymer as a chiral ligand, *Pure Appl. Chem.*, 2012, **84**, 1759–1769.
22 M. Kumar, P. Brocorens, C. Tonnelé, D. Beljonne, M. Surin and S. J. George, A dynamic supramolecular polymer with stimuli-responsive handedness for in situ probing of enzymatic ATP hydrolysis, *Nat. Commun.*, 2014, **5**, 5793.
23 A. Mishra, S. Dhiman and S. J. George, ATP-driven synthetic supramolecular assemblies: from ATP as a template to Fuel, *Angew. Chem., Int. Ed.*, 2021, **60**, 2740–2756.
24 S. Dhiman, A. Jain, M. Kumar and S. J. George, Adenosine-phosphate-fueled, temporally programmed supramolecular polymers with multiple transient states, *J. Am. Chem. Soc.*, 2017, **139**, 16568–16575.
25 A. Mishra, D. B. Korlepara, M. Kumar, A. Jain, N. Jonnalagadda, K. K. Bejagam, S. Balasubramanian and S. J. George, Biomimetic temporal self-assembly via fuel-driven controlled supramolecular polymerization, *Nat. Commun.*, 2018, **9**, 1295.
26 H. Miyake, H. Kamon, I. Miyahara, H. Sugimoto and H. Tsukube, Time-programmed peptide helix inversion of a synthetic metal complex triggered by an achiral NO^{3-} anion, *J. Am. Chem. Soc.*, 2008, **130**, 792–793.
27 C. Kulkarni, A. K. Mondal, T. K. Das, G. Grinbom, F. Tassinari, M. F. J. Mabesoone, E. W. Meijer and R. Naaman, Highly efficient and tunable filtering of electro-

ns'spin by supramolecular chirality of nanofiber-based materials, *Adv. Mater.*, 2020, **32**, 1904965.
28 C. Kulkarni, P. A. Korevaar, K. K. Bejagam, A. R. A. Palmans, E. W. Meijer and S. J. George, Solvent clathrate driven dynamic stereomutation of a supramolecular polymer with molecular pockets, *J. Am. Chem. Soc.*, 2017, **139**, 13867–13875.
29 J. Yao, W. Wu, C. Xiao, D. Su, Z. Zhong, T. Mori and C. Yang, Overtemperature-protection intelligent molecular chiroptical photoswitches, *Nat. Commun.*, 2021, **12**, 2600.
30 J. M. Lehn, A. Rigault, J. Siegel, J. Harrowfield, B. Chevrier and D. Moras, Spontaneous assembly of double-stranded helicates from oligobipyridine ligands and copper(I) cations: structure of an inorganic double helix, *Proc. Natl. Acad. Sci. U S A.*, 1987, **84**, 2565–2569.
31 A. D. Faulkner, R. A. Kaner, Q. M. A. Abdallah, G. Clarkson, D. J. Fox, P. Gurnani, S. E. Howson, R. M. Phillips, D. I. Roper, D. H. Simpson and P. Scott, Asymmetric triplex metallohelices with high and selective activity against cancer cells, *Nat. Chem.*, 2014, **6**, 797–803.
32 R. Chen, Q. Q. Yan, S. J. Hu, X. Q. Guo, L. X. Cai, D. N. Yan, L. P. Zhou and Q. F. Sun, Dinuclear helicate or mononuclear pincer lanthanide complexes from one ligand: stereo-controlled assembly and catalysis, *Org. Chem. Front.*, 2021, **8**, 2576–2582.
33 L. Wang, Z. Yao, W. Huang, T. Gao, P. Yan, Y. Zhou and H. Li, Remarkable 980 nm circularly polarized luminescence from dinuclear Yb(III) helicates with a D_4 symmetry, *Inorg. Chem. Front.*, 2023, **10**, 3664–3674.
34 F. Stomeo, C. Lincheneau, J. P. Leonard, J. E. O'Brien, R. D. Peacock, C. P. McCoy and T. Gunnlaugsson, Metal-directed synthesis of enantiomerially pure dimetallic lanthanide luminescent triple-stranded helicates, *J. Am. Chem. Soc.*, 2009, **131**, 9636–9637.
35 M. Rancan, J. Tessarolo, A. Carlotto, S. Carlotto, M. Rando, L. Barchi, E. Bolognesi, R. Seraglia, G. Bottaro, M. Casarin, G. H. Clever and L. Armelao, Adaptive helicity and chiral recognition in bright europium quadruple-stranded helicates induced by host-guest interaction, *Cell Rep. Phys. Sci.*, 2022, **3**, 100692.
36 Y. Wang, Y. Zhou, Z. Yao, W. Huang, T. Gao, P. Yan and H. Li, Asymmetric induction in quadruple-stranded europium(III) helicates and circularly polarized luminescence, *Dalton Trans.*, 2022, **51**, 10973–10982.
37 D. Zhao, T. Leeuwen, J. Cheng and B. L. Feringa, Dynamic control of chirality and self-assembly of double-stranded helicates with light, *Nat. Chem.*, 2016, **9**, 250–256.
38 H. Miyake, K. Yoshida, H. Sugimoto and H. Tsukube, Dynamic helicity inversion by achiral anion stimulus in synthetic labile cobalt(II) complex, *J. Am. Chem. Soc.*, 2004, **126**, 6524–6525.
39 X. Chen, T. M. Gerger, C. Räuber, G. Raabe, C. Göb, I. M. Oppel and M. Albrecht, A helicate-based three-state molecular switch, *Angew. Chem., Int. Ed.*, 2018, **57**, 11817–11820.
40 X. Guo, X. Zhang, S. Hu, L. Zhou and Q. Sun, Stereocontrol on lanthanide triple-stranded helicates toward enhanced enantioselective sensing, *Chem. Res. Chin. Univ.*, 2024, **40**, 842–848.
41 J. B. Maglic and R. Lavendomme, MoloVol: an easy-to-use program for analyzing cavities, volumes and surface areas of chemical structures, *J. Appl. Crystallogr.*, 2022, **55**, 1033–1044.
42 L. D. Bari, G. Pescitelli, F. Marchetti and P. Salvadori, Anomalous CD/UV exciton splitting of a binaphthyl derivative: the case of 2,2′-diiodo-1,1′-binaphthalene, *J. Am. Chem. Soc.*, 2000, **122**, 6395–6398.
43 S. G. Telfer, T. M. McLean and M. R. Waterland, Exciton coupling in coordination compounds, *Dalton Trans.*, 2011, **40**, 3097–3108.
44 J. L. Lunkley, D. Shirotani, K. Yamanari, S. Kaizaki and G. Muller, Chiroptical spectra of a series of tetrakis((+)-3-heptafluorobutylyrylcamphorato)lanthanide(III) with an encapsulated alkali metal ion: circularly polarized luminescence and absolute chiral structures for the Eu(III) and Sm(III) complexes, *Inorg. Chem.*, 2011, **50**, 12724–12732.
45 Y. Zhou, H. Li, T. Zhu, T. Gao and P. Yan, A highly luminescent chiral tetrahedral $Eu_4L_4(L')_4$ cage: chirality induction, chirality memory, and circularly polarized luminescence, *J. Am. Chem. Soc.*, 2019, **141**, 19634–19643.
46 Y. B. Tan, Y. Okayasu, S. Katao, Y. Nishikawa, F. Asanoma, M. Yamada, J. Yuasa and T. Kawai, Visible circularly polarized luminescence of octanuclear circular Eu(III) helicate, *J. Am. Chem. Soc.*, 2020, **142**, 17653–17661.
47 A. Rodger and B. Norden, *Circular dichroism and linear dichroism*, Oxford University Press, Oxford, 1997.
48 C. Lefebvre, G. Rubez, H. Khartabil, J. C. Boisson, J. C. García and E. Hénon, Accurately extracting the signature of intermolecular interactions present in the NCI plot of the reduced density gradient versus electron density, *Phys. Chem. Chem. Phys.*, 2017, **19**, 17928–17936.
49 T. Lu and Q. Chen, Independent gradient model based on Hirshfeld partition: a new method for visual study of interactions in chemical systems, *J. Comput. Chem.*, 2022, **43**, 539–555.

